Dynamics of the carbonate system in a large continental shelf system under the influence of both a river plume and coastal upwelling

Zhimian Cao,[1] Minhan Dai,[1] Nan Zheng,[1] Deli Wang,[1] Qian Li,[1] Weidong Zhai,[1] Feifei Meng,[1] and Jianping Gan[2]

Received 30 October 2010; revised 31 January 2011; accepted 10 February 2011; published 12 May 2011.

[1] We examined the dynamics of the carbonate system in a complex mixing scheme with enhanced biological consumption modulated by both a river plume and summer coastal upwelling in a large shelf system, the northern South China Sea (NSCS) shelf. The plume waters originated from a large flooding upstream the Pearl River, and extended from the mouth of the Pearl River estuary to the middle shelf and were characterized by low dissolved inorganic carbon (DIC) and total alkalinity (TAlk), and a high aragonite saturation state (Ω_{arag}). In contrast, the upwelled water occupying the nearshore area was distinguished by high DIC and TAlk and a low Ω_{arag}. While the dynamics of the carbonate system were largely shaped by physical mixing through plume and upwelling processes between the plume water, the offshore subsurface water and the offshore surface water, biological consumption of DIC was observable in both the river plume and the coastal upwelling areas and contributed to the elevated Ω_{arag} during their pathway. Correlations between salinity normalized TAlk and DIC indicated that organic carbon production rather than biocalcification exclusively induced the DIC removal. By using a three end-member mixing model, we estimated the net community productivity in the plume water and the upwelled water to be 36 ± 19 mmol C m^{-2} d^{-1} and 23 ± 26 mmol C m^{-2} d^{-1}, respectively. With the combination of stoichiometric relationship analysis of the carbonate system and applying the three end-member mixing model, we successfully differentiated semiquantitatively the biologically mediated DIC variations from its overall mixing control. We also attempted to link this natural process to the carbonate saturation on the NSCS shelf, contending that at present natural factors associated with the river plume and the coastal upwelling largely modulate the dynamics of the carbonate system on the NSCS shelf, whereas anthropogenic stressors such as ocean acidification currently play a relatively minor role.

Citation: Cao, Z., M. Dai, N. Zheng, D. Wang, Q. Li, W. Zhai, F. Meng, and J. Gan (2011), Dynamics of the carbonate system in a large continental shelf system under the influence of both a river plume and coastal upwelling, *J. Geophys. Res.*, *116*, G02010, doi:10.1029/2010JG001596.

1. Introduction

[2] Although comprising only ~7% of the world's ocean surface area, continental shelves and slopes contribute to 14–30% of the oceanic primary production (PP), ~80% of the organic matter burial and ~50% of the deposition of calcium carbonate ($CaCO_3$) [*Gattuso et al.*, 1998], establishing for them a disproportionally significant component of the global oceanic carbon cycle [*Walsh et al.*, 1981; *Rabouille et al.*, 2001; *Chen*, 2003]. Coastal seas, where various physical and biogeochemical processes interplay in a very dynamic way, are especially distinguished by two processes: river plumes and coastal upwelling.

[3] River plumes, typical of large freshwater discharges, may extend into the adjacent continental shelf hundreds of kilometers away from the estuarine mouth and become critical areas of land-ocean interaction [*Chen and Borges*, 2009; *Chen et al.*, 2010]. Continental shelves fed by large river inputs receive considerable loads of carbon, nutrients and sediments, which significantly influence the biogeochemistry of coastal seas [*Dagg et al.*, 2004; *McKee et al.*, 2004]. Both the high nutrient discharge within the river plume and the low turbidity of its lower reach are favorable for phytoplankton growth and result in enhanced biological activity [*Gaston et al.*, 2006, and references therein]. River plumes are, thus, frequently sites of phytoplankton blooms

[1]State Key Laboratory of Marine Environmental Science, Xiamen University, Xiamen, China.
[2]Division of Environment and Department of Mathematics, Hong Kong University of Science and Technology, Kowloon, Hong Kong.

0148-0227/11/2010JG001596

in coastal seas. On the other hand, coastal upwelling, resulting from prevailing upwelling-favorable winds and shelf topography, is characterized by offshore mass transport in the surface layer and onshore mass transport at depth. Upwelling brings CO_2-rich deep waters to the surface that may induce the oversaturation of CO_2 relative to the atmosphere. However, the adequate supply of nutrients from upwelling potentially stimulates the biological productivity and lowers the surface CO_2 content. Thus, the carbon dynamics in an upwelling system are complex, and largely modulated by the balance between the two opposite effects [*Borges and Frankignoulle*, 2002a, 2002b].

[4] Adding in more complexity is the interaction between the plume and upwelling, in that the wind-driven upwelling circulation can be further altered by the buoyancy from the river plume, whereas the plume itself is also shaped by the circulation over the shelf. Such plume-upwelling interaction governs nearshore circulation in a number of coastal seas [*Gan et al.*, 2009b, and references therein], but the associated biogeochemical processes are still to be elucidated.

[5] Noteworthy is that efforts have been recently devoted to examining the coastal saturation state with respect to $CaCO_3$ in the context of ocean acidification that has occurred since the last century [*Intergovernmental Panel on Climate Change*, 2007]. *Feely et al.* [2008] report the aragonite undersaturation state ($\Omega_{arag} < 1.0$) in nearshore surface waters off the Oregon-California border, due to the upwelling of corrosive "acidified" water onto the shelf area. In the Northern Gulf of Mexico, relatively high riverine total alkalinity (TAlk) together with significant biological consumption of CO_2 result in elevated Ω_{arag} values for the Mississippi plume waters [*Keul et al.*, 2010]. However, with the low TAlk input from the Kennebec River plume in the Casco Bay, Ω_{arag} values for surface waters in Gulf of Maine could be less than 1.0 [*Salisbury et al.*, 2008]. Thus, besides the organic carbon metabolism (i.e., photosynthesis/respiration), both the river plume and the coastal upwelling also affect inorganic carbon characteristics such as $CaCO_3$ saturation state and eventually the CO_2 buffer capacity of coastal seas.

[6] The South China Sea (SCS) is the world's second largest marginal sea with wide continental shelves to both the north and south. During the southwest monsoon period in the summer, coastal upwelling distributes along the coast [*Han and Ma*, 1988]. Over the shelf area in the northern SCS (NSCS), strong variability of the upwelling current exists both in alongshore and cross-shore directions due to the highly variable shelf topography [*Gan et al.*, 2009a, 2009b; *Shu et al.*, 2011]. In addition to the summer upwelling, the NSCS shelf is also featured by strong river plume waters originating from the Pearl River, a world major river system with a water discharge of 3.26×10^{11} m^3 yr^{-1}. It is noted that ~80% of the discharge takes place in the wet season (April–September) [*Su*, 2004; *Guo et al.*, 2008]. Thus, the NSCS shelf represents an important and unique system under the coinfluence of river plumes and coastal upwelling.

[7] Up to the present, phytoplankton blooms occurring in the nearshore waters of the NSCS, independently resulting from upwelling- [*Liu et al.*, 2002; *Ning et al.*, 2004] or plume-derived [*Yin et al.*, 2004; *Dai et al.*, 2008] nutrient enrichment, have been reported. The coinfluence of the two processes on the biological conditions of the NSCS shelf is, however, primarily investigated via process-oriented numerical modeling [*Gan et al.*, 2010; *Lu et al.*, 2010] or focused on relationships between sea surface pCO_2 (CO_2 partial pressure) and dissolved oxygen [*Zhai et al.*, 2009]. Studies addressing the dynamics of the carbonate system and its response to the coastal upwelling circulation and plume dynamics in the NSCS have not been reported. This study, based primarily on the examination of field data, sought to examine on how significant the river plume and the coastal upwelling may shape the dynamics of dissolved inorganic carbon (DIC) and TAlk on the NSCS shelf. We also sought to examine in a semiquantitative way the relative importance between physical mixing and biological metabolism in modulating the carbonate system in such a complex system. Finally, we were to explore how the present $CaCO_3$ saturation state (i.e., Ω_{arag}) on the NSCS shelf responds to natural processes associated with the river plume and the coastal upwelling, relative to anthropogenic stresses such as ocean acidification.

2. Materials and Methods

2.1. Study Area

[8] The NSCS, characterized by complicated coastline variations in the nearshore region, has a permanent eastward widened shelf with an offshore extension ranging from 150 to 300 km (Figure 1). In the summer, coastal upwelling occurs driven by the prevailing southwest monsoon and intensified by the widened shelf [*Gan et al.*, 2009a]. The Pearl River plume first generates a slowly expanding bulge near the mouth of the estuary, and then the freshwater in the outer part of the bulge constantly flows eastward forced by the upwelling current, resulting in a widening and thickening buoyant plume over the shelf. Meanwhile, the plume alters the upwelling circulation by accelerating the wind-driven current along the inshore edge of the plume, due to the pressure gradient between the buoyancy and the ambient seawater [*Gan et al.*, 2009b]. As a consequence, the interaction between the river plume and the coastal upwelling on the NSCS shelf significantly modulates hydrodynamic conditions, and eventually influences the biogeochemical characteristics.

[9] For instance, in the surface waters over the NSCS shelf, two distinct high-chlorophyll low-pCO_2 centers coexist during the strong southwest monsoon period [*Zhai et al.*, 2009; *Gan et al.*, 2010]. The one, over the inner shelf in the eastern part of the NSCS, results from the nutrient input of the intensified coastal upwelling, whereas the other one, over the middle shelf, is driven by the nutrient enrichment in the eastward stretched river plume. In contrast, other surface regions without the influence from either the upwelling or the plume display low chlorophyll concentration, indicating the overall oligotrophic characteristics of the SCS. In deep layers of the NSCS shelf, *Lu et al.* [2010] demonstrate the shoaling and weakening of the subsurface chlorophyll maximum (SCM) in the upwelling zone of the nearshore waters due to dilution by the low chlorophyll water upwelled from depth, while the SCM beneath the plume waters weakens, and even disappears, as a result of the substantial reduction of photosynthetic active radiation (PAR).

2.2. Cruise Background

[10] Based on the SCOPE project (South China Sea Coastal Oceanographic Process Experiment), a mapping

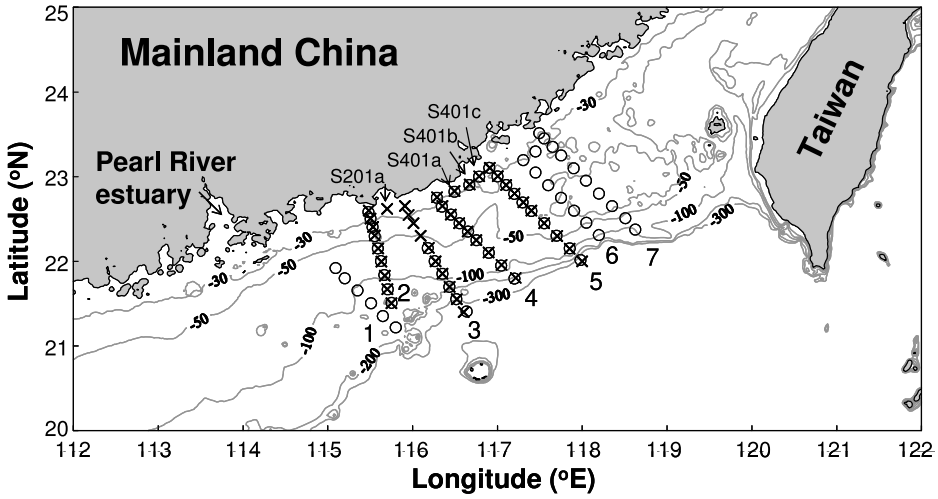

Figure 1. Map of the northern South China Sea showing its topography (in meters). Sampling stations are marked by circles for Leg 1 and by crosses for Leg 2.

cruise on board the R/V *Shiyan III* was conducted on the NSCS shelf in summer 2008. The cruise was composed of two legs. During Leg 1 from 30 June to 8 July, seven cross-shelf transects covering the region from the Pearl River estuary to east of the Taiwan Shoals (marked sequentially by numbers 1–7; Figure 1) were intensively investigated. Transects 5, 4, 3, and 2 were repeated during Leg 2 on 9–12 July. Except for Transects 1 and 3 during Leg 1, the sampling stations in each transect extended from the near-shore to the 300 m isobath and were numbered consecutively in Arabic numerals, beginning with 1 for the innermost station and increasing offshore. Along the 30 m isobath, additional stations were occupied between Transects 2 and 3 (station S201a) and between Transects 4 and 5 (stations S401a, S401b and S401c; Figure 1).

[11] As a consequence of the continuous heavy rain in the upstream Pearl River, the freshwater discharge rate reached its annual maximum ~10 days prior to our cruise, showing a very high value which was nearly double the generally observed maximum one of ~25,000 m^3 s^{-1} in the wet season (Figure 2). Resulting from such an abundant river water input, plume patches spread eastward over the NSCS shelf during Leg 1. Two low-salinity centers (typical value <29.0) were located on the inner shelf between Transects 1 and 2, and on the middle shelf at Transect 5, respectively (named as PC 1 and PC 2), whereas these centers disappeared during Leg 2 due to the subsequently weakened freshwater discharge (Figure 3). During the Leg 1 sampling period, upwelled waters characterized by low temperature (<25.0°C) and high salinity (>33.5) were distributed broadly on the inner shelf with their center located in the nearshore waters between Transects 4 and 5 (named as UC 1). However, coastal upwelling retreated to a much smaller area during Leg 2, whereas a new upwelling center outcropped in the

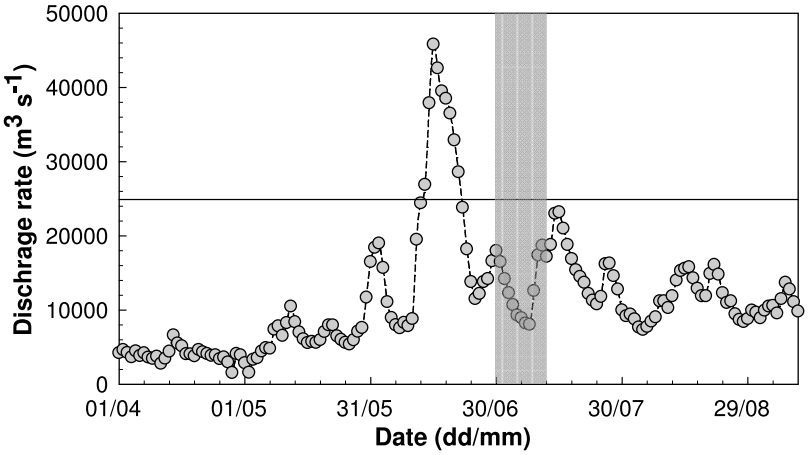

Figure 2. Freshwater discharge rate during the wet season in 2008 from the Wuzhou gauging station on the West River, the largest tributary contributing to ~70% of the total freshwater discharge of the Pearl River (China Bureau of Hydrology, Ministry of Water Resources, http://sqqx.hydroinfo.gov.cn/websq/). The gray bar indicates values during the sampling period, and the solid line shows the generally observed maximum value in the wet season.

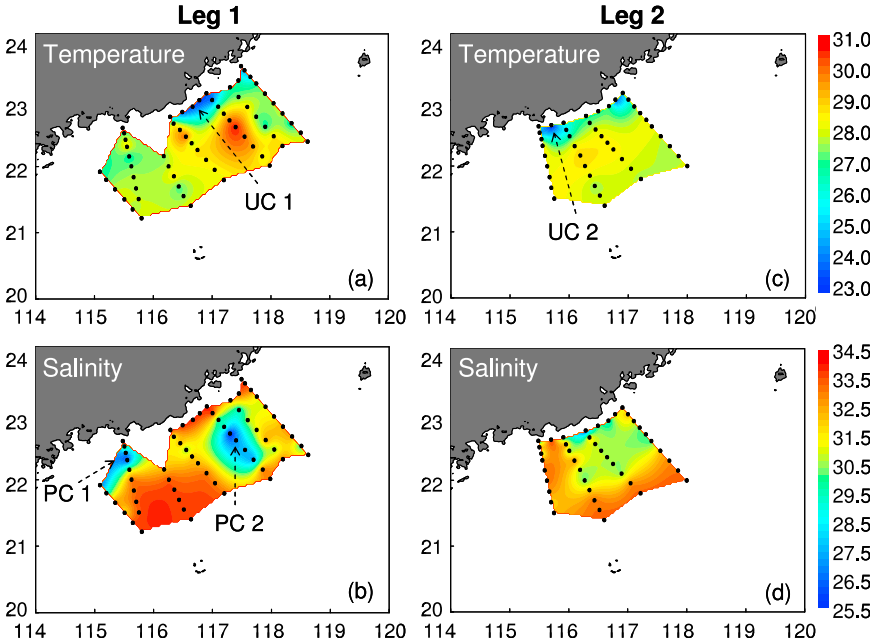

Figure 3. Surface distribution of temperature (°C) and salinity on the northern South China Sea shelf in summer 2008. (a) Leg 1: temperature; (b) Leg 1: salinity; (c) Leg 2: temperature; (d) Leg 2: salinity. PC and UC denote the plume center and the upwelling center, respectively. PC 1 involved surface waters of stations S202, S203, and S204, while PC 2 involved that of stations S505, S506, and S507. UC 1 was composed of surface waters from the five nearshore stations between Transects 4 and 5, while UC 2 was composed of that from stations S201, S201a, and S301.

nearshore waters between Transects 2 and 3 (named as UC 2), which was previously occupied by freshwater during Leg 1 (Figure 3).

2.3. Sampling and Analysis

[12] During the cruise, high spatial resolution measurements of the carbonate chemistry through the whole water column were performed. Samples were collected with Niskin bottles attached on a Rosette sampler. Samples for DIC and TAlk analysis were stored in 40 mL borosilicate glass vials and 100 mL polyethylene bottles, respectively. Both DIC and TAlk samples were poisoned using an $HgCl_2$-saturated solution upon sample collection, with 50 μL for DIC and 100 μL for TAlk. Samples for pH were free of bubbles and stored in a thermostat (25.0°C) for ~30 min before their measurement on board. Filtered samples for dissolved calcium ion (Ca^{2+}) analysis were stored in 60 mL acid-cleaned polyethylene bottles with Parafilm wrapped around the cap.

[13] Depth profiles of temperature and salinity were determined shipboard with a calibrated SBE-19-plus Conductivity-Temperature-Depth (CTD) recorder (Sea-Bird Co.) [*Shu et al.*, 2011]. DIC and TAlk data were collected both during the cruise and within a week after the cruise. DIC was determined by acidification of 0.5 mL of a water sample and the subsequent quantification of CO_2 with a nondispersive IR detector (Li-Cor 7000). TAlk was determined using Gran titration on a 25 mL sample with a Kloehn digital syringe pump. Each method has a precision of ±2 μmol kg^{-1} [*Cai et al.*, 2004]. Both DIC and TAlk were calibrated against the certified reference material provided by A. Dickson of the Scripps Institution of Oceanography. pH was determined using a Orion 3 Star pH Benchtop analyzer and a Orion Ross combined pH electrode, which was calibrated against three NIST-traceable pH buffers (pH 4.01, 7.00 and 10.01). Precision of pH measurements was ±0.005. The in situ pH values (pH_{NIST}) were calculated based on an empirical temperature calibrating equation ($pH^{in\ situ} = pH^{meas} + 0.0114 \times (T^{meas} - T^{in\ situ})$, where $pH^{in\ situ}$ and pH^{meas} are the pH values at the in situ temperature ($T^{in\ situ}$) and at the measurement temperature (T^{meas}), respectively [*Gieskes*, 1969]). Ca^{2+} was determined in the onshore laboratory using the EGTA titration with a Methrom 809 TITRANDO potentiometer, which has a precision of better than ±5 μmol kg^{-1} [*Cao and Dai*, 2011].

2.4. Calculation of Other Carbonate System Parameters

[14] DIC and TAlk data were applied to the program CO2SYS [*Lewis and Wallace*, 1998] to calculate pH_{SW} (in seawater scale), carbonate ion (CO_3^{2-}) concentration and fugacity of CO_2 (fCO_2). The dissociation constants for carbonic acid (K_1 and K_2) were those of *Mehrbach et al.* [1973] refitted by *Dickson and Millero* [1987], and K_{HSO4} was determined by *Dickson* [1990]. To obtain Ω_{arag} ($\Omega = [Ca^{2+}][CO_3^{2-}]/K_{sp}$), the solubility product (K_{sp}) for aragonite was taken from *Mucci* [1983], and Ca^{2+} concentrations were estimated from the in situ Ca^{2+}/salinity relationship ($Ca^{2+} = 273 \times Salinity + 675$, n = 163, r = 0.99) for the NSCS shelf of this study.

[15] The calculated pH_{SW} values had an offset of ~0.15 lower than those of pH_{NIST}. This offset is common due to

the measurement uncertainty induced by the different ion strength between the NIST buffers and seawater samples [*Dickson*, 1984]. As pH_{SW} represents the true value of seawater and for direct comparison with pH values in other studies employing seawater scale [e.g., *Feely et al.*, 2008], we used pH_{SW} throughout this study. The calculated surface fCO_2 agreed well with that obtained from underway measurements during the cruise (Q. Li et al., unpublished data, 2010). The systematic deviation was ±5 μatm.

2.5. Regional Salinity Normalization

[16] To differentiate the biological/chemical effects from those of physical processes on the marine carbonate system, normalization to a constant salinity (usually a salinity of 35 or the average salinity of filed data) is commonly applied to the DIC, TAlk and Ca^{2+} data. However, such normalization assumes that salinity changes are only due to the freshwater removal by evaporation or addition by rain precipitation with zero solutes, which is clearly not true on the NSCS shelf with a large river plume. This study thus adopted an approach of regional normalization [*Friis et al.*, 2003] using a nonzero freshwater end-member as:

$$NX = \frac{X^{meas} - X^{S=0}}{S^{meas}} \times S^{ref} + X^{S=0} \quad (1)$$

[17] In equation (1), NX and X^{meas} are normalized and measured values for DIC, TAlk or Ca^{2+}. S^{meas} is the CTD measured salinity. S^{ref} is the reference salinity, which is defined as the average salinity value in this study. $X^{S=0}$ is the end-member value for DIC, TAlk or Ca^{2+} at a salinity of 0, which is the intercept of the linear regression line between surface measured X and salinity.

2.6. TAlk Versus DIC

[18] The apparent relationship between TAlk and DIC has been used for a long time to differentiate water masses undergoing various biological activities and their mixing [*Broecker and Peng*, 1982]. The two main biological processes involving changes of DIC and TAlk in seawaters can be illustrated as in the following equations:
Organic carbon metabolism (photosynthesis/respiration)

$$106CO_2 + 122H_2O + 16HNO_3 + H_3PO_4 \leftrightarrow (CH_2O)_{106}(NH_3)_{16}H_3PO_4 + 138O_2 \quad (2)$$

Inorganic carbon metabolism ($CaCO_3$ production/dissolution)

$$Ca^{2+} + 2HCO_3^- \leftrightarrow CaCO_3 + CO_2 + H_2O \quad (3)$$

[19] During photosynthesis the change in TAlk with decrease in DIC is minor (−17 versus 106), dependent on the uptake of nutrients, which gives a TAlk/DIC change ratio of −0.16. On the other hand, DIC decreases by 1 mol and TAlk by 2 moles per mole $CaCO_3$ production, resulting in the TAlk/DIC change ratio being equal to 2. Thus, the slope of the linear regression line between NTAlk and NDIC after removing the physical effect can be used to assess the relative importance of the organic and inorganic carbon metabolism in a fixed water parcel [*Robertson et al.*, 1994; *Gattuso et al.*, 1996; *Cao et al.*, 2009].

3. Results

3.1. Surface Distribution of DIC, TAlk, and Ω_{arag}

[20] Surface regions occupied by fresher waters displayed distinguishable low DIC and TAlk (Figure 4). Waters with the lowest DIC and TAlk content (lower than ~1740 and ~2010 μmol kg^{-1}, respectively) were located at PC 1 and PC 2 during Leg 1, whereas during Leg 2 both values of PC 2 were higher with more increase in TAlk, suggesting weakening of the plume during Leg 2. It should be noted that, with the high nutrient supply, the plume-induced bloom might further decrease DIC and/or TAlk through enhanced biological productivity. Due to the fact that deep waters are replete in DIC and TAlk, surface regions occupied by upwelled waters (UC 1 and UC 2) were characterized by high DIC and TAlk (higher than ~1940 and ~2210 μmol kg^{-1}, respectively; Figure 4), which were comparable to, or even higher than, those in the outer shelf surface seawater.

[21] All surface Ω_{arag} values, within the range 2.3 and 3.9, were higher than 1.0, suggesting an aragonite oversaturation state in the surface waters of the NSCS shelf (Figure 4). During Leg 1, waters with the highest Ω_{arag} of ~3.8 were located in PC 2 while the Ω_{arag} values for the waters in PC 1 were slightly lower. The lowest Ω_{arag} of ~2.7 were observed in UC 1, where coastal upwelling brought more corrosive subsurface water to the surface. Surface Ω_{arag} values during Leg 2 were overall higher than those of Leg 1, except for UC 2. With an extremely low Ω_{arag} value of ~2.3 in UC 2, offshore subsurface waters were elevated and finally outcropped to the nearshore surface between Transects 2 and 3 during Leg 2.

3.2. Vertical Distribution of DIC, TAlk, and Ω_{arag}

[22] As distinguished by the physico-chemical properties of the river plume or the coastal upwelling or the combination of both during different sampling periods, vertical structures of the carbonate system along Transects 2 and 5 were selected (Figure 5). DIC, TAlk and Ω_{arag} distributions in Transect 2 displayed overall stratification during Leg 1. The buoyant water in the top 10 m of the inner shelf, characterized by low DIC (~1800 μmol kg^{-1}) and TAlk (~2080 μmol kg^{-1}) and relatively high Ω_{arag} (~3.0), formed a relatively strong gradient along the plume and at the bottom. However, all DIC, TAlk, and Ω_{arag} contours of Transect 2 during Leg 2 tilted upward abruptly toward the shore. CO_2-rich waters from a depth of ~150 m (DIC > 2050 μmol kg^{-1} and $\Omega_{arag} < 2.0$) increased along the upward sloping seafloor and outcropped to the shallow inner shelf, which was previously covered by freshwater (Figure 5).

[23] During Leg 1, the typical plume contours of DIC (~1800 μmol kg^{-1}) and TAlk (~2080 μmol kg^{-1}) moved to the middle shelf in Transect 5 and deepened, suggesting that the plume moved eastward over the NSCS shelf and thickened on its offshore side. It should be noted that during the transport of the plume water, Ω_{arag} values increased from ~3.0 to ~3.8, displaying the most aragonite oversaturated state. Moreover, this offshore plume in Transect 5 was separated from both the inner shelf water containing upwelled

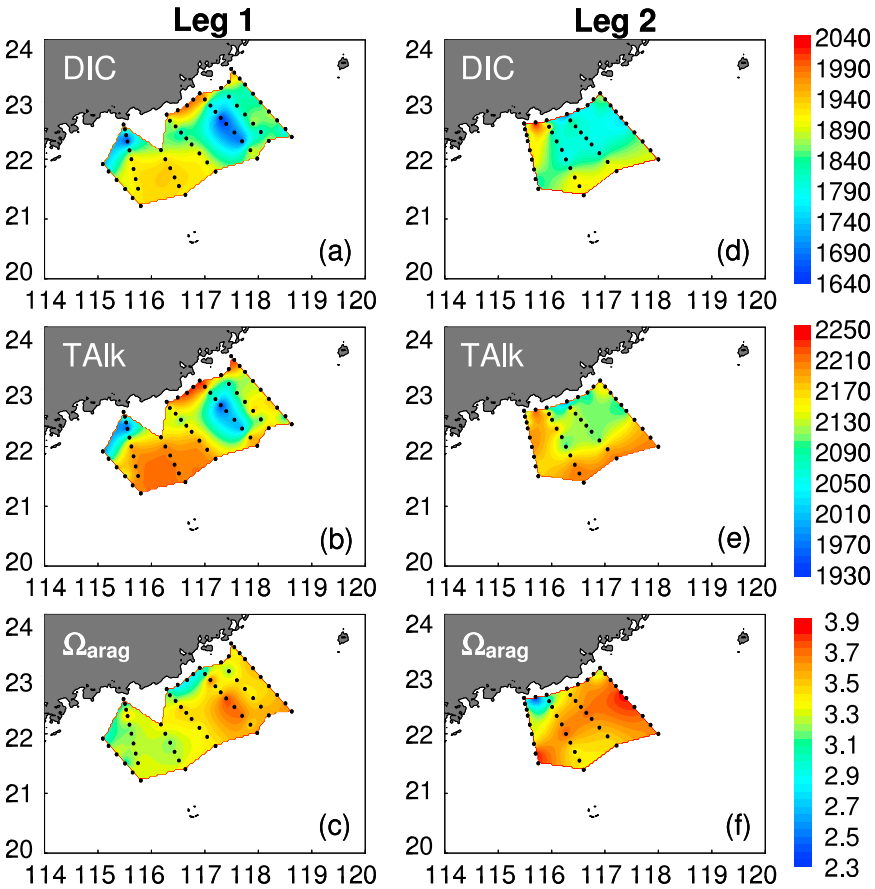

Figure 4. Surface distribution of DIC (μmol kg^{-1}), TAlk (μmol kg^{-1}), and Ω_{arag} on the northern South China Sea shelf in summer 2008. (a) Leg 1: DIC; (b) Leg 1: TAlk; (c) Leg 1: Ω_{arag}; (d) Leg 2: DIC; (e) Leg 2: TAlk; (f) Leg 2: Ω_{arag}.

subsurface waters and the outer shelf surface water (Figure 5). The TAlk pattern of the top 20 m waters in Transect 5 during Leg 2 suggested that signals from both the river plume and the coastal upwelling were weakened. However, low DIC concentrations along Transect 5 were observed at greater depth relative to Leg 1, corresponding with deepened Ω_{arag} contours in the top 50 m waters.

4. Discussion

[24] Both surface and vertical distribution of DIC, TAlk and Ω_{arag} suggested that the dynamics of the carbonate system on the NSCS shelf in summer were largely controlled by the mixing of different water masses sourced from the plume, the subsurface water upwelled and the offshore surface water. The apparent relationship between DIC and TAlk (Figure 6) further confirmed the significant control of the three end-member mixing scheme. Abundant data points were distributed along two mixing lines, one between the plume water of lowest DIC and TAlk and the offshore surface water, and the other one between the offshore surface water and the offshore subsurface water of highest DIC and TAlk. It should also be noted that some of the data points were located on the mixing line between the offshore subsurface water and the plume water, indicating the occurrence of coastal upwelling (Figure 6). *Gan et al.* [2010] demonstrate enhanced biological productivity in two algal blooms on the NSCS shelf, which were induced by the large nutrient supply from the river plume and the coastal upwelling, respectively. As major reactants involved in photosynthesis and/or biocalcification (equations (2) and (3)), the response of DIC and TAlk to varied biological activities and the resultant Ω_{arag} variation on the NSCS shelf are scrutinized below.

4.1. DIC and TAlk Response to the River Plume

[25] Along the plume pathway (from PC 1 to PC 2), both DIC and TAlk values displayed no difference, whereas DIC values beneath the top freshwater were lower in PC 2 than PC 1 but TAlk remained the same (Figure 7a). However, NDIC values were much lower in PC 2 corresponding with a relatively higher pH_{SW} (Figures 7b and 7c), suggesting strong biological uptake of DIC during the plume transport. NTAlk values still displayed no difference between PC 1 and PC 2, and their surface values were nearly identical with those of the deep waters after regional salinity normalization (Figure 7b), suggesting the predominant control of physical mixing on the TAlk distribution.

[26] As shown in Figure 8a, NDIC variations (~30 μmol kg^{-1} maximum) in both PC 1 and PC 2 were much larger than those of NTAlk (~5 μmol kg^{-1} maximum), whereas the average NDIC value was ~40 μmol kg^{-1} lower in PC 2 than PC 1. Both slopes of the linear regression line between NTAlk and NDIC in PC 1 and PC 2 agreed well with the

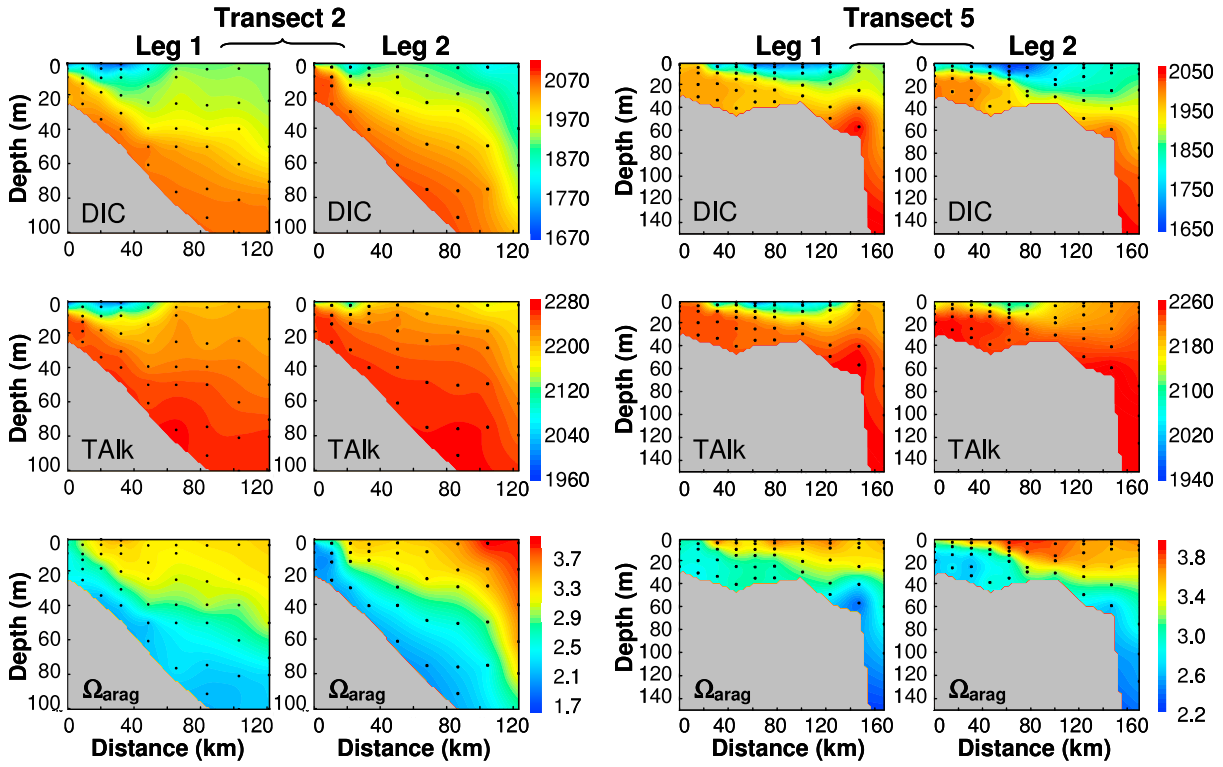

Figure 5. Vertical distribution of (top) DIC (μmol kg^{-1}), (middle) TAlk (μmol kg^{-1}), and (bottom) Ω_{arag} along (left) Transect 2 and (right) Transect 5 on the northern South China Sea shelf in summer 2008. Data collected during Leg 1 and Leg 2 are shown.

theoretical value of −0.16 deduced from the organic carbon metabolism (equation (2)). The significant DIC removal on the pathway of the plume should have resulted exclusively from the enhanced organic carbon production. Moreover, surface Ca^{2+} and salinity displayed good positive linear relationship whereas NCa^{2+} maintained a nearly constant value despite variations in salinity (Figure 8b). The conservative Ca^{2+} behavior further suggested that the biogenic $CaCO_3$ production or dissolution be ruled out in the surface waters of the region and therefore had a negligible influence on DIC and TAlk. It should also be noted that in such a short timescale as several days for plume water transport, the effect of air-sea exchange of CO_2 could be neglected relative to the biological activity [*Borges and Frankignoulle*, 2002a; *Zhai et al.*, 2009]. The slope value of nearly −0.16 (Figure 8a) further indicated the negligible influence of air-sea exchange of CO_2 on DIC variations, during which the TAlk/DIC change ratio equals 0.

4.2. DIC and TAlk Response to Coastal Upwelling

[27] Vertical distribution of DIC and TAlk from stations involved in UC 1 and UC 2 were relatively uniform throughout the water column (Figure 9), suggesting the dominance of upwelled subsurface waters. Unlike TAlk/NTAlk which displayed no great difference among stations involved in UC 1, DIC/NDIC decreased gradually from station S401 to station S501 corresponding with a northward increasing trend in pH_{SW} (Figure 9a). Although DIC displayed less variation among the stations involved in UC 2 relative to UC 1, a northward decreasing trend still existed corresponding with the increasing pH_{SW} (Figure 9b). *Gan et al.* [2009b] propose that upwelled waters off Shanwei (the position of UC 2) are subsequently transported northward and then outcropped off Shantou (the position of UC 1). Note that NTAlk concentrations from all stations were

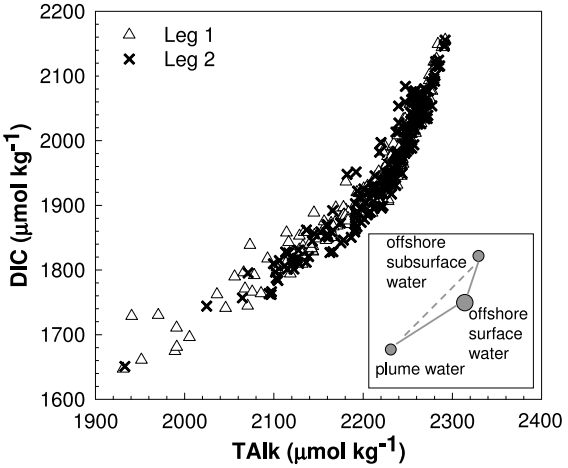

Figure 6. DIC versus TAlk on the northern South China Sea shelf in summer 2008. The inset shows the schematic mixing processes. The solid circles represent three major source waters. The solid lines show general water mixing among the plume water, the offshore surface water, and the offshore subsurface water, while the dashed line shows water mixing during the coastal upwelling observed in this study.

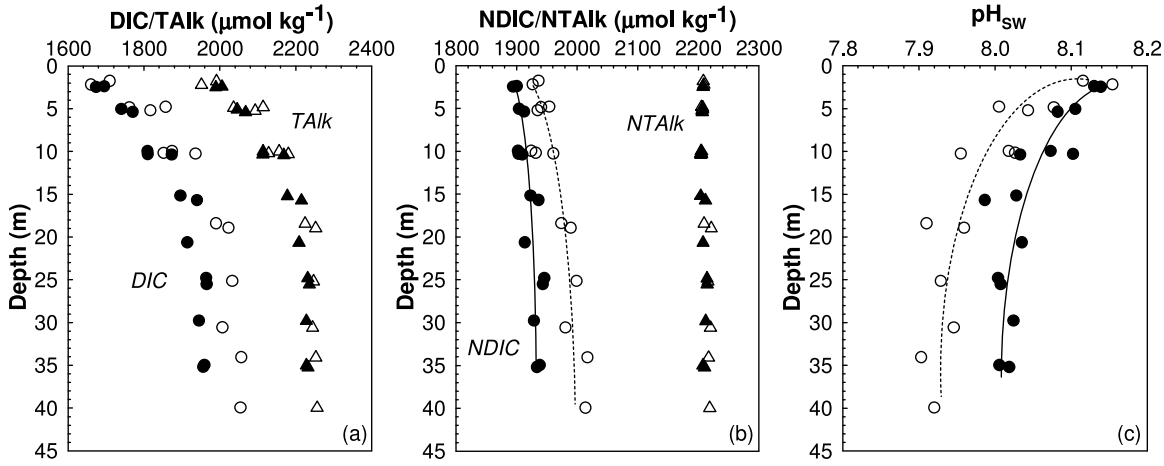

Figure 7. Vertical profiles of three carbonate system parameters in plume centers (PC) and the water beneath. (a) DIC and TAlk; (b) NDIC and NTAlk; (c) pH_{SW}. The open symbols represent data in PC 1 including stations S202, S203, and S204, while the solid symbols are for data in PC 2 including stations S505, S506, and S507 (Figure 3). N denotes the salinity normalized value.

nearly constant, which might suggest that the same water mass occupied the whole nearshore area from UC 2 to UC 1. However, the average NDIC value from stations involved in UC 1 was ~50 μmol kg^{-1} lower than that of UC 2 while pH_{SW} values were much higher (Figure 9). Together with the observed northward decreasing trend of NDIC during different sampling periods, we contend that DIC was consumed gradually during the transport of the upwelled water in the nearshore area of the NSCS shelf.

[28] As shown in Figure 10a, NDIC variations (~30 μmol kg^{-1} maximum) in both stations S401 and S501 involved in UC 1 were much larger than those of NTAlk (~6 μmol kg^{-1} maximum), whereas the average NDIC value was ~35 μmol kg^{-1} lower in station S501 than in station S401. Although data points employed in Figure 10a were not abundant, and statistically, uncertainties associated with the slope estimates could be large such as the scenario for station S401, both slopes of the linear regression line within the limit of uncertainties were close to the theoretical value of −0.16 deduced from the organic carbon metabolism (equation (2)). The significant DIC removal during transport of the upwelled water should exclusively have resulted from the enhanced organic carbon production. Moreover, Ca^{2+} collected from the upwelled water correlated well with salinity whereas NCa^{2+} values were nearly constant despite variations in salinity, suggesting its conservative behavior (Figure 10b). Similar to the scenario of the river plume, the biogenic $CaCO_3$ production or dissolution as well as the air-sea exchange of CO_2 apparently had little influence on either DIC or TAlk in the upwelled waters.

4.3. Biologically Mediated DIC Variations Estimated Using a Three End-Member Mixing Model

[29] We adopted a three end-member mixing model to quantitatively evaluate the biologically mediated DIC variations in both the river plume and the coastal upwelling.

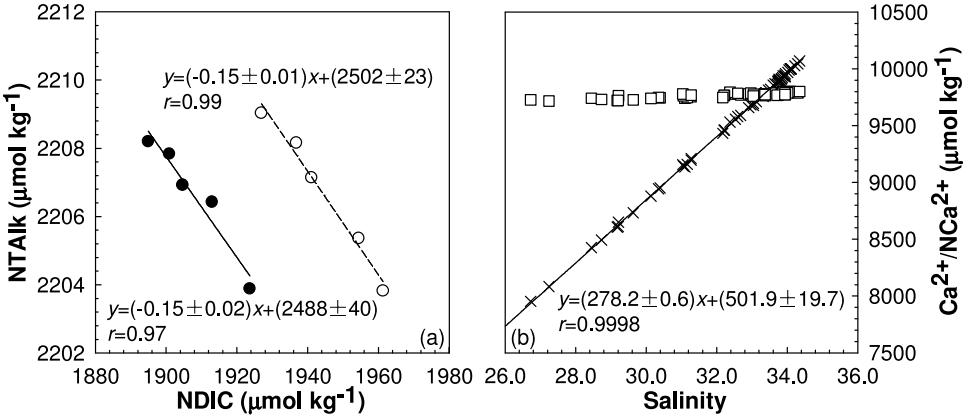

Figure 8. (a) NTAlk versus NDIC in the plume centers (PC). The open symbols represent data in PC 1 including stations S202, S203, and S204, while the solid symbols are for data in PC 2 including stations S505, S506, and S507 (Figure 3). (b) Surface Ca^{2+} (crosses) and NCa^{2+} (squares) versus salinity. Data were collected from the top 10 m of water of the SCOPE domain. N denotes the salinity normalized value.

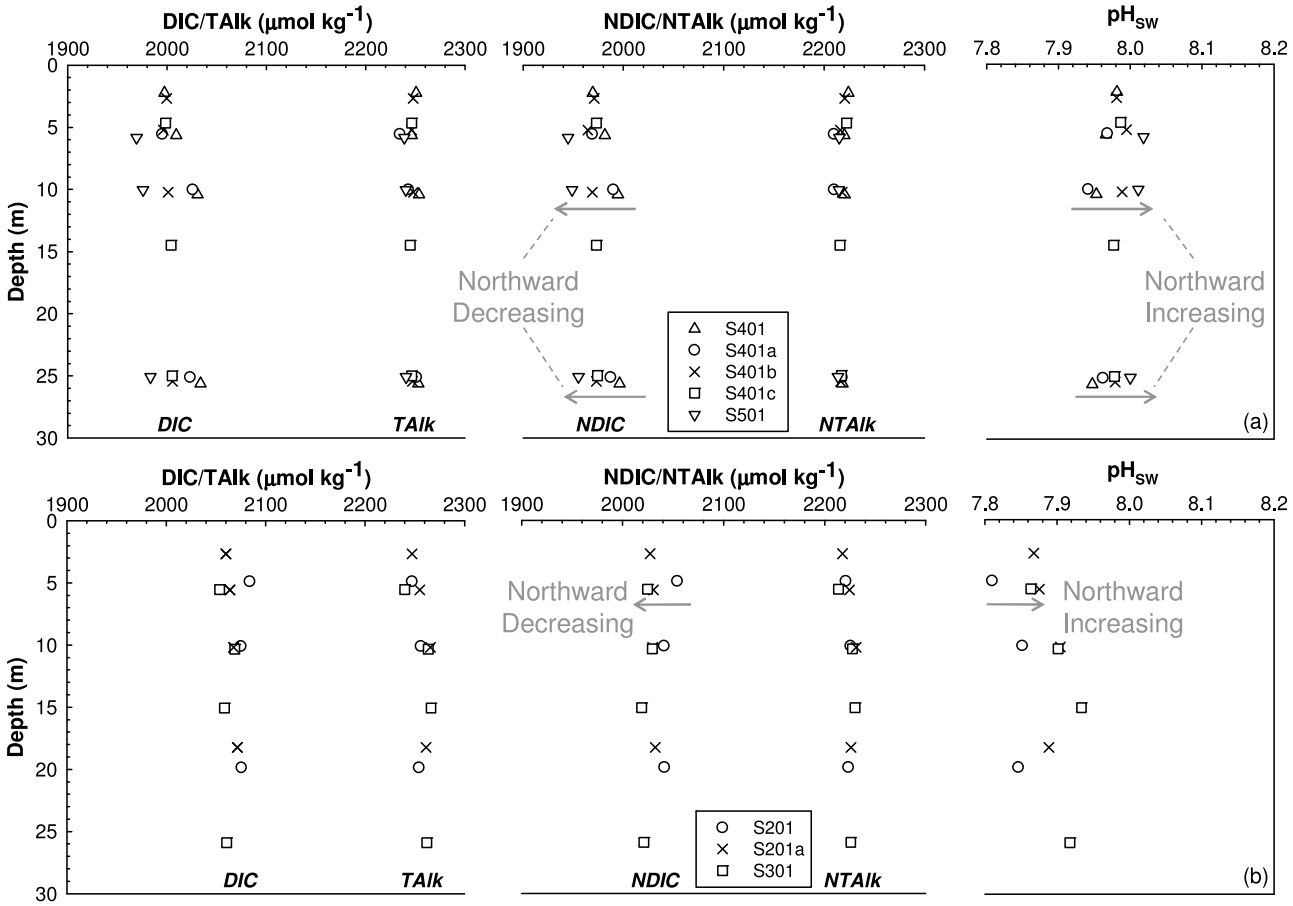

Figure 9. Vertical profiles of DIC/TAlk, NDIC/NTAlk, and pH_{SW} in nearshore upwelled waters. (a) Stations involved in UC 1 during Leg 1. (b) Stations involved in UC 2 during Leg 2 (Figure 3). UC denotes the upwelling center, and N denotes the salinity normalized value.

The thermohaline properties of any sample were the sum of the contribution of the three end-members [*Álvarez-Salgado et al.*, 1997], which can be calculated using equations (4)–(6):

$$F_p + F_u + F_s = 1 \tag{4}$$

$$\theta_p F_p + \theta_u F_u + \theta_s F_s = \theta_{spl} \tag{5}$$

$$S_p F_p + S_u F_u + S_s F_s = S_{spl} \tag{6}$$

where F_p, F_u and F_s are the respective fractions of the plume water, the offshore subsurface water and the offshore surface water in the water sample. θ_p, θ_u and θ_s are the potential temperatures of the three end-member waters; while S_p, S_u and S_s denote the salinity of the end-members. θ_{spl} and S_{spl} are the potential temperature and salinity of the water sample.

[30] The conservative DIC concentrations (DIC°) resulting from the mixing of the three end-members can be calculated using equation (7):

$$DIC^{\circ} = DIC_p F_p + DIC_u F_u + DIC_s F_s \tag{7}$$

where DIC_p, DIC_u and DIC_s are the DIC concentrations of the three end-member waters.

[31] The difference between the conservative and measured concentration (ΔDIC in equation (8)) which is not accounted for by the model, represents the influence of other processes with positive values indicating DIC removal and negative ones suggesting its addition.

$$\Delta DIC = DIC^{\circ} - DIC_{spl} \tag{8}$$

[32] Table 1 summarizes the end-member values employed in the model during different sampling periods. For comparison between Leg 1 and Leg 2, only data from Transects 2 to 5 were applied to the model.

4.3.1. ΔDIC in the River Plume

[33] Plume water is defined as water with salinity <33.0 over the shelf [*Gan et al.*, 2010]. The positive ΔDIC values during both Leg 1 and Leg 2 indicated the exclusively biological removal of DIC in the river plume. The ΔDIC displayed an overall trend decreasing with the increasing salinity, suggesting stronger biological activities in lower salinity waters abundant in plume waters (Figure 11). Although the influence from the river plume apparently weakened during Leg 2, the average ΔDIC value of 33 ± 15 μmol kg^{-1} was nearly the same as that of Leg 1 (32 ± 18 μmol kg^{-1}). The plume-delivered nutrients should continuously stimulate biological productivity to the same extent throughout the whole sampling period. Together with the mixed layer depth of ~13 m and a radium-estimated residence time of ~12 days for plume waters on the NSCS shelf (data not shown), we estimated that the net community production (NCP) for the river plume was 36 ± 19 mmol

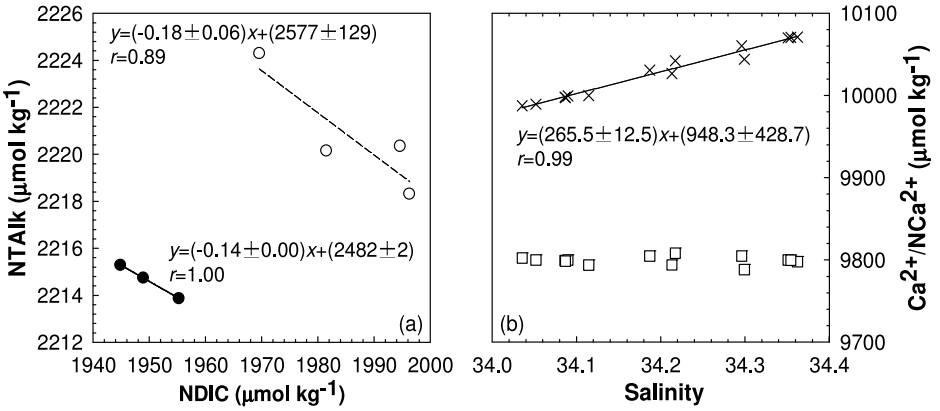

Figure 10. (a) NTAlk versus NDIC from stations S401 (open symbols) and S501 (solid symbols) involved in UC 1 (Figure 3); (b) Ca^{2+} (crosses) and NCa^{2+} (squares) versus salinity. Data were collected from the whole water column involved in UC 1 (stations S401, S401b, and S501; Figure 3) and UC 2 (station S301; Figure 3). UC denotes the upwelling center, and N denotes the salinity normalized value.

C m^{-2} d^{-1}. This NCP value was comparable to the plume's PP of 35–50 mmol C m^{-2} d^{-1} estimated using a model [*Gan et al.*, 2010], which was reasonably close to or slightly higher than NCP dependent on the extent of organic matter degradation in the plume [*Cai et al.*, 2004].

[34] The NCP value in the present study was much lower than another plume event in May 2001 on the NSCS shelf (70–110 mmol C m^{-2} d^{-1} [*Dai et al.*, 2008]). It should be noted that the location of the plume-induced bloom observed by *Dai et al.* [2008] was limited to nearshore at the mouth of the Pearl River estuary, whereas significant DIC removal extended to the far reaches of the plume in the present study. Thus, we contend that such an episodic event as being demonstrated in summer 2008 might have contributed to the coastal carbon budgets on a larger temporal and spatial scale.

4.3.2. ΔDIC in the Coastal Upwelling

[35] Upwelled water is defined as water with salinity > 33.75 in the nearshore upper 20 m [*Gan et al.*, 2010]. Over half of ΔDIC values were negative, indicating overall DIC addition during the upwelling process (Figure 12). The added DIC might originate from the remineralization of particulate organic matter (POM) in the onshore-flowing water at depth [*Álvarez-Salgado et al.*, 1997]. However, ΔDIC increased generally from Transects 2 to 5 during both Leg 1 and Leg 2, and positive values were observed on the inner shelf of Transect 5 (Figure 12). The added DIC should be consumed rapidly through enhanced organic carbon production during the northward transport of the upwelled water in the nearshore area of the NSCS shelf (i.e., from Shanwei to Shantou). Thus, the biologically mediated DIC variation corresponding to the coastal upwelling consisted of two components: (1) net DIC release via POM degradation in the near-bottom onshore-flowing water and (2) net DIC uptake after the subsurface water outcropped and was transported in the nearshore area, where PAR was available for organic carbon production.

[36] Although ΔDIC values in the upwelled waters during Leg 2 were overall lower than those of Leg 1, both gradients of ΔDIC between Transects 2 and 5 were ~80 μmol kg^{-1} (Figure 12). The upwelling-delivered nutrients should stimulate the biological productivity to the same extent during different sampling periods. For stations involved

Table 1. Summary of End-Member Values During Leg 1 and Leg 2 of the Cruise in Summer 2008 to the Northern South China Sea Shelf[a]

	Leg 1			Leg 2		
	θ (°C)	S	DIC (μmol kg^{-1})	θ (°C)	S	DIC (μmol kg^{-1})
Plume water	27.0	24.5	1710	28.6	27.5	1740
Offshore surface water	28.6	33.7	1920	28.6	33.7	1900
Offshore subsurface water	17.0	34.5	2100	17.0	34.6	2120

[a]Here θ and S denote potential temperature and salinity.

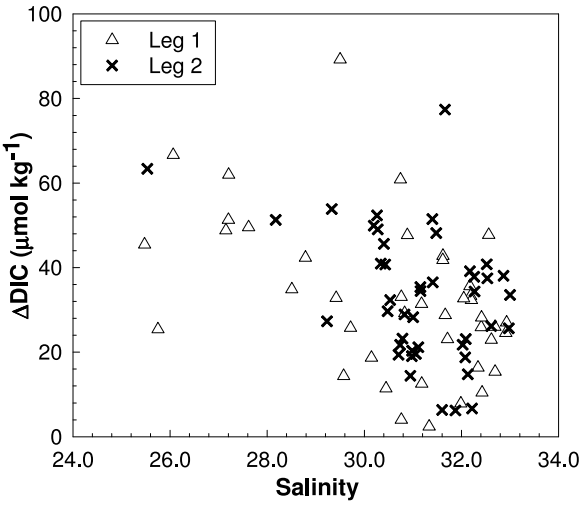

Figure 11. ΔDIC versus salinity for the plume water between Transects 2 and 5 on the northern South China Sea shelf in summer 2008. ΔDIC represents the biologically mediated DIC variations (equation (8)).

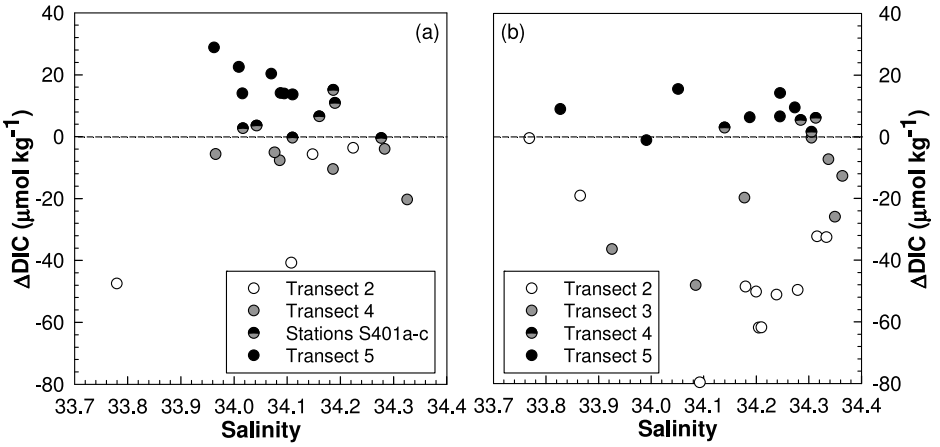

Figure 12. ΔDIC versus salinity for the upwelled water between Transects 2 and 5 on the northern South China Sea shelf in summer 2008. (a) Leg 1; (b) Leg 2. ΔDIC represents the biologically mediated DIC variations (equation (8)).

in UC1 during the entire sampling period (Figure 3), the average ΔDIC value was 8 ± 9 μmol kg^{-1}. Together with the surface water depth of ~20 m and a radium-estimated residence time of ~7 days (data not shown), we estimated that the NCP for upwelled waters on the NSCS shelf was 23 ± 26 mmol C m^{-2} d^{-1}. Despite the large uncertainty, this NCP value agreed well with the model-simulated PP value of 10–30 mmol C m^{-2} d^{-1} within the upwelled water [*Gan et al.*, 2010].

4.3.3. Comparison Between Plume and Upwelling

[37] Within the uncertainties of the simple model, NCP values for the plume water were slightly higher than or comparable to those for the upwelled water. *Gan et al.* [2010] also simulate lower surface productivity in the upwelling

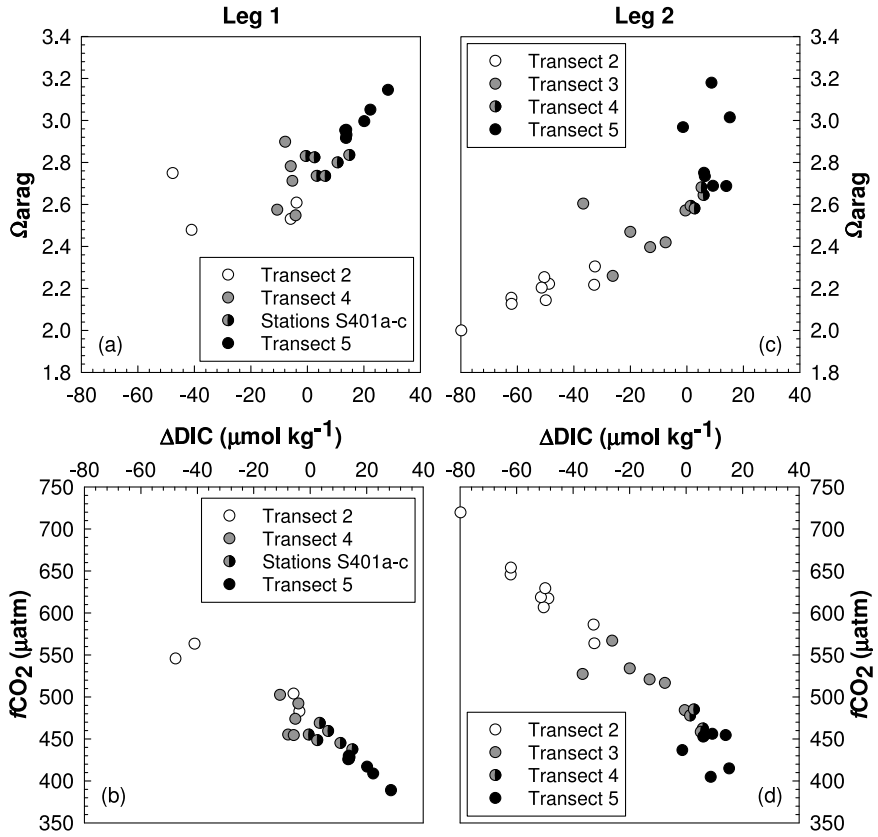

Figure 13. Ω_{arag} and fCO_2 versus ΔDIC for the upwelled water between Transects 2 and 5 on the northern South China Sea shelf in summer 2008. (a) Leg 1: Ω_{arag} versus ΔDIC; (b) Leg 1: fCO_2 versus ΔDIC; (c) Leg 2: Ω_{arag} versus ΔDIC; (d) Leg 2: fCO_2 versus ΔDIC. ΔDIC represents the biologically mediated DIC variations (equation (8)).

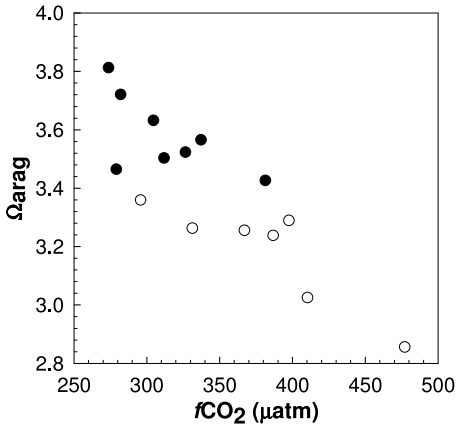

Figure 14. Ω_{arag} versus fCO_2 in the plume centers (PC). The open symbols represent data in PC 1 including stations S202, S203, and S204, while the solid symbols are for data in PC 2 including stations S505, S506, and S507 (Figure 3).

relative to the plume, but the difference decreases gradually during the maturation of the biological system. Moreover, enhanced biological production with significant nutrient removal was also observed in subsurface waters, due to the uplifting of the nutricline during intensified upwelling (A. Q. Han et al., Nutrient dynamics and biological consumption in a large continental shelf system under the influence of both a river plume and coastal upwelling, manuscript in preparation, 2011). While the coastal upwelling fueled the overall productivity, the Pearl River plume injected a relatively higher level to the surface of the NSCS shelf.

4.4. Ω_{arag} Controlling Mechanisms

[38] The overall lowest Ω_{arag} values in UC 1 and UC 2 were largely imprints of upwelled subsurface corrosive waters, which were enriched with both anthropogenic CO_2 and natural process induced CO_2 (e.g., POM degradation). During the northward transport of the upwelled water, however, Ω_{arag} increased whereas fCO_2 decreased with increasing ΔDIC during both Leg 1 and Leg 2 (Figure 13). The consistent biological production gradually consumed CO_2 and raised CO_3^{2-}, resulting in the increasing Ω_{arag} pattern in the upwelled water.

[39] Due to the fact that the TAlk concentration of the Pearl River plume was relatively low (Figure 4), the high Ω_{arag} in the plume water could not have originated from the abundant CO_3^{2-} load of the freshwater. Actually, Ω_{arag} values for PC 1 were comparable to those of the surrounding normal NSCS surface waters (Figure 4). However, Ω_{arag} values for PC 2 were distinguishably higher during Leg 1. From PC 1 to PC 2, Ω_{arag} increased from ~3.0 to ~3.8 whereas fCO_2 decreased by ~200 μatm. The overall negative relationship between Ω_{arag} and fCO_2 indicated that biological uptake of CO_2 was the primary determinant of Ω_{arag} within the plume water on the NSCS shelf (Figure 14).

[40] In addition, surface Ω_{arag} values were overall elevated during Leg 2 relative to Leg 1 (Figure 4), while Ω_{arag} contours with high values deepened during Leg 2 (e.g., Transect 5 during Leg 2; Figure 5). The enhanced biological production via nutrient enrichment, either from the river plume or the coastal upwelling, raised Ω_{arag} generally through the whole sampling period. By simulating the decadal changes of the carbonate system in the Belgian coastal zone, *Borges and Gypens* [2010] demonstrate a positive relationship between PP and Ω_{arag} and contend that the increased PP due to eutrophication could counter the effects of ocean acidification on the surface carbonate chemistry in coastal environments. Although focusing on much shorter timescale events, our study provided another piece of evidence that natural processes related to nutrient delivery should primarily control the carbonate system in coastal seas, whereas ocean acidification might play a relatively minor role.

5. Concluding Remarks

[41] Our observations of DIC and TAlk on the NSCS shelf during an upwelling wet season have demonstrated that the dynamics of the carbonate system were jointly controlled by physical and biological forcings associated with a river plume and coastal upwelling. Biologically mediated DIC consumption was obvious within the plume system through enhanced organic carbon production, corresponding to a NCP of 36 ± 19 mmol C m^{-2} d^{-1}. Such DIC removal was also observed in the upwelling regime with however complicated scenarios dependent upon the timing and locations. Addition of DIC via POM degradation in the near-bottom onshore-flowing water was likely, whereas subsequent DIC removal occurred after the offshore subsurface water outcropped and was transported in the nearshore area. The estimated NCP for the upwelled water was 23 ± 26 mmol C m^{-2} d^{-1}, which was almost comparable to the plume water. The three end-member mixing model has proven to be efficient to estimate at least semiquantitatively relative importance between physical mixing and biological activities in a complex circulation scheme often encountered in river influenced marginal systems.

[42] All Ω_{arag} values were higher than 1.0, suggesting that ocean acidification currently plays a minor role in lowering the $CaCO_3$ saturation state on the NSCS shelf. The contrasting scenarios between the present system and the continental shelf off Oregon [*Feely et al.*, 2008] might be related to the different "acidity" of source waters of upwelling. In the latter case, offshore subsurface waters from ~150 m with $\Omega_{arag} < 1.0$ and $pH_{SW} < 7.75$ upwell to surface nearshore [*Feely et al.*, 2008]. In our system, probably also true for most of the upwelling systems on wide shelves, the upwelled subsurface water has a significantly higher Ω_{arag} value of ~1.9 and pH_{SW} value of ~7.95 despite also being sourced from the depth of ~150 m. On the other hand, the enhanced biological consumption of CO_2 induced elevated Ω_{arag} within both the plume and upwelled waters. The patterns of Ω_{arag} observed on the NSCS shelf are largely controlled by natural circulation and biological activities at present. However, with more anthropogenic CO_2 accumulation, undersaturated waters with $\Omega_{arag} < 1.0$ may be possible in this local marine ecosystem in the future. Based on the conceptual diagram proposed in the study of *Feely et al.* [2010], further work is warranted to understand and predict variations of the $CaCO_3$ saturation state and CO_2 buffer capacity in such coastal seas, especially under the coinfluence of anthropogenic stressors such as ocean acidification and natural factors including river inputs and upwelling.

[43] **Acknowledgments.** This study was financially supported by the National Basic Research Program of China (973 Program) through grant 2009CB421201, and by the National Science Foundation of China (NSFC) through grants 90711005 and 40821063 and NSFC-RGC project (grants 40731160624 and N_HKUST623/07). The sampling cruise was supported by the SCOPE project coorganized by Jiang Zhu, Dongxiao Wang, Xiaogang Guo, Minhan Dai, and Jianping Gan. We would like to thank Xiaoqing Xie, Minquan Guo, Yuancheng Su, Yan Yang, Zongpei Jiang, and Xianghui Guo for help with the ancillary data collection and the crew of *Shiyan III* for their assistance in sample collection. We thank Dongxiao Wang and Jianyu Hu for providing the CTD data and John Hodgkiss for his help with English.

References

Álvarez-Salgado, X. A., C. G. Castro, F. F. Pérez, and F. Fraga (1997), Nutrient mineralization patterns in shelf waters of the Western Iberian upwelling, *Cont. Shelf Res.*, *17*, 1247–1270.

Borges, A. V., and M. Frankignoulle (2002a), Aspects of dissolved inorganic carbon dynamics in the upwelling system off the Galician coast, *J. Mar. Syst.*, *32*, 181–198.

Borges, A. V., and M. Frankignoulle (2002b), Distribution of surface carbon dioxide and air-sea exchange in the upwelling system off the Galician coast, *Global Biogeochem. Cycles*, *16*(2), 1020, doi:10.1029/2000GB001385.

Borges, A. V., and N. Gypens (2010), Carbonate chemistry in the coastal zone responds more strongly to eutrophication than to ocean acidification, *Limnol. Oceanogr.*, *55*(1), 346–353.

Broecker, W. S., and T.-H. Peng (1982), *Tracers in the Sea*, 690 pp., Lamont-Doherty Earth Observatory, Palisades, N. Y.

Cai, W.-J., M. Dai, Y. Wang, W. Zhai, T. Huang, S. Chen, F. Zhang, Z. Chen, and Z. Wang (2004), The biogeochemistry of inorganic carbon and nutrients in the Pearl River estuary and the adjacent Northern South China Sea, *Cont. Shelf Res.*, *24*, 1301–1319.

Cao, Z. M., and M. H. Dai (2011), Shallow-depth $CaCO_3$ dissolution: Evidence from excess calcium in the South China Sea and its export to the Pacific Ocean, *Global Biogeochem. Cycles*, doi:10.1029/2009GB003690, in press.

Cao, Z. M., M. H. Dai, Z. M. Lu, and K. B. Zhou (2009), $CaCO_3$ to organic carbon ratio in the South China Sea, in *Advances in Geosciences*, vol. 12, *Ocean Science*, edited by J. P. Gan et al., World Sci., Hackensack, N. J.

Chen, C. T. A. (2003), New vs. export production on the continental shelf, *Deep Sea Res., Part II*, *50*, 1327–1333.

Chen, C. T. A., and A. V. Borges (2009), Reconciling opposing views on carbon cycling in the coastal ocean: Continental shelves as sinks and near-shore ecosystems as sources of atmospheric CO_2, *Deep Sea Res., Part II*, *56*, 578–590.

Chen, C. T. A., S. Jan, T. H. Huang, and Y. H. Tseng (2010), Spring of no Kuroshio intrusion in the southern Taiwan Strait, *J. Geophys. Res.*, *115*, C08011, doi:10.1029/2009JC005804.

Dagg, M., R. Benner, S. Lohrenz, and D. Lawrance (2004), Transformation of dissolved and particulate materials on continental shelves influenced by large rivers: Plume processes, *Cont. Shelf Res.*, *24*, 833–858.

Dai, M. H., et al. (2008), Effects of an estuarine plume-associated bloom on the carbonate system in the lower reaches of the Pearl River estuary and the coastal zone of the northern South China Sea, *Cont. Shelf Res.*, *28*(12), 1416–1423.

Dickson, A. G. (1984), pH scales and proton-transfer reactions in saline media such as sea water, *Geochim. Cosmochim. Acta*, *48*, 2299–2308.

Dickson, A. G. (1990), Standard potential of ($AgCl(s) + 1/2\ H_2(g) = Ag(s) + HCl(aq)$) cell and the dissociation constant of bisulfate ion in synthetic seawater from 273.15 to 318.15 K, *J. Chem. Thermodyn.*, *22*, 113–127.

Dickson, A. G., and F. J. Millero (1987), A comparison of the equilibrium constants for the dissociation of carbonic acid in seawater media, *Deep Sea Res.*, *34*, 1733–1743.

Feely, R. A., C. L. Sabine, J. M. Hernandez-Ayon, D. Ianson, and B. Hales (2008), Evidence for upwelling of corrosive "acidified" water onto the continental shelf, *Science*, *320*, 1490–1492.

Feely, R. A., S. R. Alin, J. Newton, C. L. Sabine, M. Warner, A. Devol, C. Krembs, and C. Maloy (2010), The combined effects of ocean acidification, mixing, and respiration on pH and carbonate saturation in an urbanized estuary, *Estuarine Coastal Shelf Sci.*, *88*, 442–449.

Friis, K., A. Körtzinger, and D. W. R. Wallace (2003), The salinity normalization of marine inorganic carbon chemistry data, *Geophys. Res. Lett.*, *30*(2), 1085, doi:10.1029/2002GL015898.

Gan, J. P., A. Cheung, X. G. Guo, and L. Li (2009a), Intensified upwelling over a widened shelf in the northeastern South China Sea, *J. Geophys. Res.*, *114*, C09019, doi:10.1029/2007JC004660.

Gan, J. P., L. Li, D. X. Wang, and X. G. Guo (2009b), Interaction of a river plume with coastal upwelling in the northeastern South China Sea, *Cont. Shelf Res.*, *29*, 728–740.

Gan, J., Z. Lu, M. Dai, A. Y. Y. Cheung, H. Liu, and P. Harrison (2010), Biological response to intensified upwelling and to a river plume in the northeastern South China Sea: A modeling study, *J. Geophys. Res.*, *115*, C09001, doi:10.1029/2009JC005569.

Gaston, T. F., T. A. Schlacher, and R. M. Connolly (2006), Flood discharges of a small river into open coastal waters: Plume traits and material fate, *Estuarine Coastal Shelf Sci.*, *69*, 4–9.

Gattuso, J.-P., M. Pichon, B. Delesalle, C. Canon, and M. Frankignoulle (1996), Carbon fluxes in coral reefs. I. Lagrangian measurement of community metabolism and resulting air-sea CO_2 disequilibrium, *Mar. Ecol. Prog. Ser.*, *145*, 109–121.

Gattuso, J.-P., M. Frankignoulle, and R. Wollast (1998), Carbon and carbonate metabolism in coastal aquatic ecosystems, *Annu. Rev. Ecol. Syst.*, *29*, 405–434.

Gieskes, J. M. (1969), Effect of temperature on the pH of seawater, *Limnol. Oceanogr.*, *14*, 679–685.

Guo, X. H., W.-J. Cai, W. D. Zhai, M. H. Dai, Y. C. Wang, and B. S. Chen (2008), Seasonal variations in the inorganic carbon system in the Pearl River (Zhujiang) estuary, *Cont. Shelf Res.*, *28*, 1424–1434.

Han, W. Y., and K. M. Ma (1988), Studies on the coastal upwelling along the coasts of the east Guangdong Province, (in Chinese), *Acta Oceanogr. Sin.*, *10*(1), 52–59.

Intergovernmental Panel on Climate Change (2007), Summary for policymakers, in *Climate Change 2007: The Physical Science Basis. Contribution of Working Group I to the Fourth Assessment Report of the Intergovernmental Panel on Climate Change*, edited by S. Solomon et al., pp. 1–18, Cambridge Univ. Press, New York.

Keul, N., J. W. Morse, R. Wanninkhof, D. K. Gledhill, and T. S. Bianchi (2010), Carbonate chemistry dynamics of surface waters in the northern Gulf of Mexico, *Aquat. Geochem.*, *16*, 337–351.

Lewis, E., and D. W. R. Wallace (1998), Program developed for CO_2 system calculations, *ORNL/CDIAC-105*, Carbon Dioxide Inf. Anal. Cent., Oak Ridge Natl. Lab., U.S. Dep. of Energy, Oak Ridge, Tenn.

Liu, K.-K., S.-Y. Chao, P.-T. Shaw, G.-C. Gong, C.-C. Chen, and T. Y. Tang (2002), Monsoon-forced chlorophyll distribution and primary production in the South China Sea: Observations and a numerical study, *Deep Sea Res., Part I*, *49*, 1387–1412.

Lu, Z. M., J. P. Gan, M. H. Dai, and A. Y. Y. Cheuang (2010), The influence of coastal upwelling and a river plume on the subsurface chlorophyll maximum over the shelf of the northeastern South China Sea, *J. Mar. Syst.*, doi:10.1016/j.jmarsys.2010.03.002.

McKee, B. A., R. C. Aller, M. A. Allison, T. S. Bianchi, and G. C. Kineke (2004), Transport and transformation of dissolved and particulate materials on continental margins influenced by major rivers: Benthic boundary layer and seated processes, *Cont. Shelf Res.*, *24*, 899–926.

Mehrbach, C., C. H. Culberson, J. E. Hawley, and R. N. Pytkowicz (1973), Measurement of the apparent dissociation constants of carbonic acid in seawater at atmospheric pressure, *Limnol. Oceanogr.*, *18*, 897–907.

Mucci, A. (1983), The solubility of calcite and aragonite in seawater at various salinities, temperatures, and one atmosphere total pressure, *Am. J. Sci.*, *283*, 780–799.

Ning, X., F. Chai, H. Xue, Y. Cai, C. Liu, and J. Shi (2004), Physical-biological oceanographic coupling influencing phytoplankton and primary production in the South China Sea, *J. Geophys. Res.*, *109*, C10005, doi:10.1029/2004JC002365.

Rabouille, C., F. T. Mackenzie, and L. M. Ver (2001), Influence of the human perturbation on carbon, nitrogen, and oxygen biogeochemical cycles in the global coastal ocean, *Geochim. Cosmochim. Acta*, *65*, 3615–3641.

Robertson, J. E., C. Robinson, D. R. Turner, P. Holligan, A. J. Watson, P. Boyd, E. Fernandez, and M. Finch (1994), The impact of a coccolithophore bloom on oceanic carbon uptake in the northeast Atlantic during summer 1991, *Deep Sea Res., Part I*, *41*, 297–314.

Salisbury, J., M. Green, C. Hunt, and J. Campbell (2008), Coastal acidification by rivers: A threat to shellfish?, *Eos Trans. AGU*, *89*(50), doi:10.1029/2008EO500001.

Shu, Y., D. Wang, J. Zhu, and S. Peng (2011), The 4-D structure of upwelling and Pearl River plume in the northern South China Sea during summer 2008 revealed by a data assimilation model, *Ocean Modell.*, doi:10.1016/j.ocemod.2011.01.002.

Su, J. (2004), Overview of the South China Sea circulation and its influence on the coastal physical oceanography outside the Pearl River Estuary, *Cont. Shelf Res.*, *24*, 1745–1760.

Walsh, J. J., G. T. Rowe, R. L. Iverson, and C. P. McRoy (1981), Biological export of shelf carbon is a sink of the global CO_2 cycle, *Nature*, *291*, 196–201.

Yin, K. D., P. Y. Qian, J. C. Chen, D. P. H. Hsieh, and P. J. Harrison (2004), Dynamics of nutrients and phytoplankton biomass in the Pearl River estuary and adjacent waters of Hong Kong during summer: Preliminary evidence for phosphorus and silicon limitation, *Mar. Ecol. Prog. Ser.*, *194*, 295–305.

Zhai, W. D., M. H. Dai, and W.-J. Cai (2009), Coupling of surface pCO_2 and dissolved oxygen in the northern South China Sea: Impacts of contrasting coastal processes, *Biogeosciences*, *6*, 2589–2598.

Z. Cao, M. Dai, Q. Li, F. Meng, D. Wang, W. Zhai, and N. Zheng, State Key Laboratory of Marine Environmental Science, Xiamen University, 422 Simingnanlu, Xiamen 361005, China. (mdai@xmu.edu.cn)

J. Gan, Department of Mathematics, Hong Kong University of Science and Technology, Kowloon, Hong Kong.